

# The effect of hydrodynamical simulation inspired dark matter velocity profile on directional detection of dark matter

Ranjan Laha<sup>1</sup>

<sup>1</sup>*Kavli Institute for Particle Astrophysics and Cosmology (KIPAC),  
Department of Physics, Stanford University, Stanford, CA 94305, USA  
SLAC National Accelerator Laboratory, Menlo Park, CA 94025, USA  
ranjalah@uni-mainz.de*

(Dated: March 4, 2022)

Directional detection is an important way to detect dark matter. An input to these experiments is the dark matter velocity distribution. Recent hydrodynamical simulations have shown that the dark matter velocity distribution differs substantially from the Standard Halo Model. We study the impact of some of these updated velocity distribution in dark matter directional detection experiments. We calculate the ratio of events required to confirm the forward-backward asymmetry and the existence of the ring of maximum recoil rate using different dark matter velocity distributions for  $^{19}\text{F}$  and  $\text{Xe}$  targets. We show that with the use of updated dark matter velocity profiles, the forward-backward asymmetry and the ring of maximum recoil rate can be confirmed using a factor of  $\sim 2 - 3$  less events when compared to that using the Standard Halo Model.

## I. INTRODUCTION

Despite the overwhelming astrophysical evidence for dark matter, particle physics signatures of dark matter are still lacking [1–4]. There are various ways to detect dark matter particle candidates with masses  $\text{GeV} \lesssim m_\chi \lesssim \text{TeV}$ . Direct detection, indirect detection, and collider searches form the three-prong approach to detect dark matter particles in this mass range [5–7].

Among these three search strategies, direct detection of dark matter is the only way to detect local dark matter particles [8]. These searches typically proceed via the detection of  $\sim \mathcal{O}(\text{keV})$  nuclear recoils. Due to the enormous background at these energies, it is extremely difficult to distinguish the dark matter signal from background. In past, dark matter signals have been claimed by some of these searches, however, none of these have stood further detailed scrutiny [9–13].

In order to separate signal from background, it was pointed out some time ago to utilize the directional nature of the scattering of dark matter particle with nuclei [14]. The motion of the Solar system through the Galaxy will produce a distinct angular recoil spectrum [15–29]. It is expected that background will not produce such an angular recoil spectrum.

There are numerous ongoing directional dark matter detection experiments, for e.g., DRIFT [30, 31], D3 [32, 33], DMTPC [34–36], NEWAGE [37, 38], and MIMAC [39, 40]. All these experiments need to reconstruct a track of length  $\sim \mathcal{O}(\text{mm})$ . All these gaseous targets have a small target mass, and scaling up to a sizable target mass is also an enormous challenge [41–44]. Recently, there have been suggestions to use dense Xenon gas as a target for directional dark matter detection, but the research and development in that direction is still in a very nascent stage [45–48].

In addition to the forward-backward asymmetry, a ring like feature can also be used as an efficient

discriminator between signal and background in a dark matter directional detection experiment [49]. The ring corresponds to the angle at which the angular recoil rate is the maximum. The angular recoil rate has a maximum at the “ring angle” and falls off at angles away from it, and this maximum rate appears as a ring (due to the azimuthal symmetry of the scattering) when viewed in 3 dimensions. This feature prominently appears for a dark matter particle masses  $\gtrsim 100 \text{ GeV}$ , and for a low nuclear recoil threshold [49]. Due to the importance of this feature, it is imperative to check the robustness of this feature for various different dark matter velocity distributions. The ring feature is also present for bound state dark matter “darkonium” and the conclusions in this work apply qualitatively for it too [26, 50].

In this work, we investigate the forward-backward asymmetry and the ring for updated dark matter velocity profiles. Recent hydrodynamical dark matter simulations have shown that the Milky Way dark matter velocity profile deviates from the Standard Halo Model (SHM) [51–54]. The impact of these velocity profiles on non-directional dark matter searches have been considered recently [54–57]. Current constraints on dark matter - nucleon scattering cross section from directional detection experiments are quite weak. We estimate the ratios of the number of events required to reach  $3\sigma$  discrimination in forward-backward asymmetry and the appearance of a ring for various different velocity profiles. Using the ratio makes our result independent of the uncertainties due to the dark matter local density, and the dark matter - nucleon cross section. We remind the reader that in this work, we are only explore the magnitude of the dark matter velocity, i.e., the speed distribution. We use the word “velocity” following convention.

We show our results for two targets:  $^{19}\text{F}$  and  $\text{Xe}$ . Although other targets are also used in directional

detection, our choice is representative, and bracket the uncertainty due to different nuclear targets.

The remaining part of the work is arranged as follows. In Section II, we introduce the various dark matter velocity profiles, and recapitulate the necessary formulas for dark matter directional detection. We present our results in Sec. III, and conclude in Sec. IV.

## II. CALCULATIONS

### A. Dark matter velocity profile

The typical dark matter velocity profile used is the standard halo model:

$$f(v) \propto \frac{1}{(2\pi\sigma_v^2)^{3/2}} e^{-v^2/2\sigma_v^2}, \quad (1)$$

where  $\sigma_v = 155.59 \text{ km s}^{-1}$ . This analytical velocity model arises from the assumption of an isothermal dark matter density profile. The dark matter velocity in the inertial Galactocentric frame is denoted by  $v$ . The escape velocity is assumed to be  $v_{\text{esc}} \sim 600 \text{ km s}^{-1}$  [58]. Hydrodynamical simulations which include baryons give a different dark matter velocity profile. Recently, Milky Way like halos from the EAGLE HR [59, 60] and APOSTLE IR [61, 62] simulations were fit to four different dark matter velocity profiles:

(1) standard Maxwellian distribution:

$$f(v) \propto v^2 \exp[-(v/v_0)^2], \quad (2)$$

(2) generalized Maxwellian distribution:

$$f(v) \propto v^2 \exp[-(v/v_0)^{2\alpha}], \quad (3)$$

(3) velocity distribution advocated by Mao et al. [63]:

$$f(v) \propto v^2 \exp[-v/v_0] (v_{\text{esc}}^2 - v^2)^p \Theta(v_{\text{esc}} - v), \quad (4)$$

and (4) velocity distribution advocated by Lisanti et al. [64]:

$$f(v) \propto v^2 \exp[(v_{\text{esc}}^2 - v^2)/(kv_0^2 - 1)]^k \Theta(v_{\text{esc}} - v). \quad (5)$$

The criteria for the selection of Milky Way like halos from the simulations were: (i) agreement with the observed Milky Way rotation curve, (ii) stellar mass similar to the Milky Way:  $4.5 \times 10^{10} M_{\odot} < M_* < 8.3 \times 10^{10} M_{\odot}$ , and (iii) the presence of a stellar disc [65]. There were 14 halos which fit the first two criteria, and only two halos, E9 and E11, fit all the criteria. In general, all of these halos are better fit by the Mao et al. velocity profile. We concentrate on the standard Maxwellian and the Mao et al. velocity profiles as derived for the two halos: E9 and E11. The parameters are:

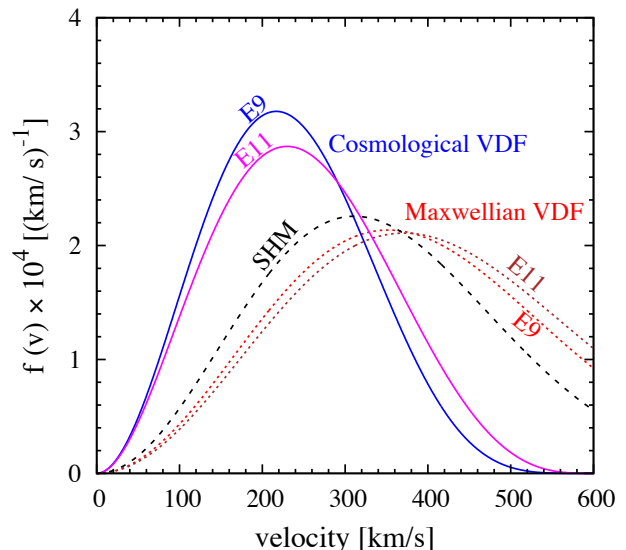


FIG. 1. The Milky Way dark matter velocity profiles considered in this work. The Standard Halo Model is labelled as SHM. The standard Maxwellian velocity distribution (eqn. 2) fits to halos E9 and E11 are labelled as Maxwellian VDF. The Mao et al. velocity distribution (eqn. 4) fits to halos E9 and E11 are labelled as Cosmological VDF.

(i) E9: standard Maxwellian  $v_0 = 248.81 \text{ km s}^{-1}$ ; Mao et al.  $v_0 = 393.63 \text{ km s}^{-1}$ , and  $p = 4.82$ ,

(ii) E11: standard Maxwellian  $v_0 = 262.27 \text{ km s}^{-1}$ ; Mao et al.  $v_0 = 250.06 \text{ km s}^{-1}$ , and  $p = 3.14$ .

These velocity profiles are shown in Fig. 1. We denote the standard Maxwellian velocity distribution function as Maxwellian VDF, and the Mao et al. velocity distribution function as Cosmological VDF. For comparison, the standard halo model is also shown as SHM. The Maxwellian VDF deviates substantially from the Cosmological VDF for both the halos E9 and E11. This is a reflection of the poor reduced  $\chi^2$  for the Maxwellian VDF for both these halos. In spite of the poor fit, we include the Maxwellian VDF to broadly encompass the uncertainties in the dark matter velocity profile.

### B. Dark matter directional detection

The formalism for dark matter directional detection is well known. Here we recapitulate the main ideas for completeness. The double differential rate ( $R$ ) w.r.t. the nuclear recoil energy ( $E_{\text{nr}}$ ) and solid angle ( $\Omega$ ) of a dark matter particle colliding with a nucleus is given by [26]

$$\frac{d^2 R}{dE_{\text{nr}} d\Omega} = N_T n_{\chi} \int d^3 \mathbf{v} f(v) \times \frac{\sigma_A^{\text{SD}} F_{\text{SD}}^2(E_{\text{nr}}) m_A}{4\pi \mu^2} \delta\left(\mathbf{v} \cdot \hat{\mathbf{q}} - \frac{q}{2\mu}\right), \quad (6)$$

where  $N_T$  denotes the number of target nuclei, the local number density of dark matter particles is denoted by  $n_\chi$ ,  $\sigma_A^{\text{SD}}$  denotes the spin-dependent dark matter - nucleon cross section,  $F_{\text{SD}}^2$  denotes the spin-dependent nuclear form factor,  $m_A$  denotes the mass of the target nuclei,  $\mu$  denotes the reduced mass of the dark matter - nucleus system,  $\mathbf{v}$  is the dark matter velocity vector in the Galactic frame,  $\mathbf{q}$  denotes the nuclear recoil direction vector with  $\hat{\mathbf{q}}$  being the corresponding unit vector. We have chosen the spin-dependent cross section in this expression as traditionally directional detection experiments show constraints for this interaction. This choice has little effect on the main results presented in the paper. Recent theoretical work has also considered the effect of dark matter effective operators on the various directional features in a dark matter experiment [66, 67].

Transforming this expression to the laboratory frame gives us

$$\frac{d^2 R}{dE_{\text{nr}} d\Omega_{v_{E}q}} = N_T n_\chi \int_{v_E \cos \theta_{v_{E}q} + q/2\mu}^{v_{\text{max}}} \frac{\sigma_A^{\text{SD}} F_{\text{SD}}^2(E_{\text{nr}}) m_A}{4\pi \mu^2} \times 2\pi v f(v) dv, \quad (7)$$

where  $\Omega_{v_{E}q}$  denotes that the solid angle is between the velocity of the Earth and the nuclear recoil direction, and  $v_{\text{max}}$  denotes the maximum velocity of the dark matter particles. When the dark matter velocity distribution follows the standard Maxwellian velocity distribution, the above mentioned equation can be integrated exactly to obtain

$$\frac{d^2 R}{dE_{\text{nr}} d\Omega_{v_{E}q}} = N_T n_\chi \frac{\sigma_A^{\text{SD}} F_{\text{SD}}^2(E_{\text{nr}}) m_A}{4\pi \mu^2} \times 2\pi N v_0^2 \left( e^{-\frac{(v_E \cos \theta_{v_{E}q} + q/2\mu)^2}{2v_0^2}} - e^{-\frac{v_{\text{max}}^2}{2v_0^2}} \right), \quad (8)$$

where the speed of the Earth w.r.t. the Galaxy is denoted by  $v_E$ . The normalization constant for the velocity distribution is denoted by  $N = 1/4\pi \times 1/(N_1 + N_2)$ , where

$$N_1 = -v_{\text{max}} v_0^2 \exp\left(-\frac{v_{\text{max}}^2}{2v_0^2}\right), \quad (9)$$

$$N_2 = \sqrt{\frac{\pi}{2}} v_0^3 \operatorname{erf}\left(\frac{v_{\text{max}}}{\sqrt{2}v_0}\right), \quad (10)$$

where erf denotes the error function.

Both the forward-backward asymmetry and the ring-like structure can be understood as a competition between the two exponential functions in eqn. 8. For the dark matter masses that we consider and the  $^{19}\text{F}$  nuclei, the values of  $\mu$  varies from  $\sim 16$  GeV to  $\sim 18.6$  GeV. For the dark matter masses that we consider and the Xe nuclei, the values of  $\mu$  varies from  $\sim 56.3$  GeV to  $\sim 115.8$  GeV. For the recoil energies that we consider, the recoil momentum of the  $^{19}\text{F}$  nuclei falls between  $\sim 13.7$

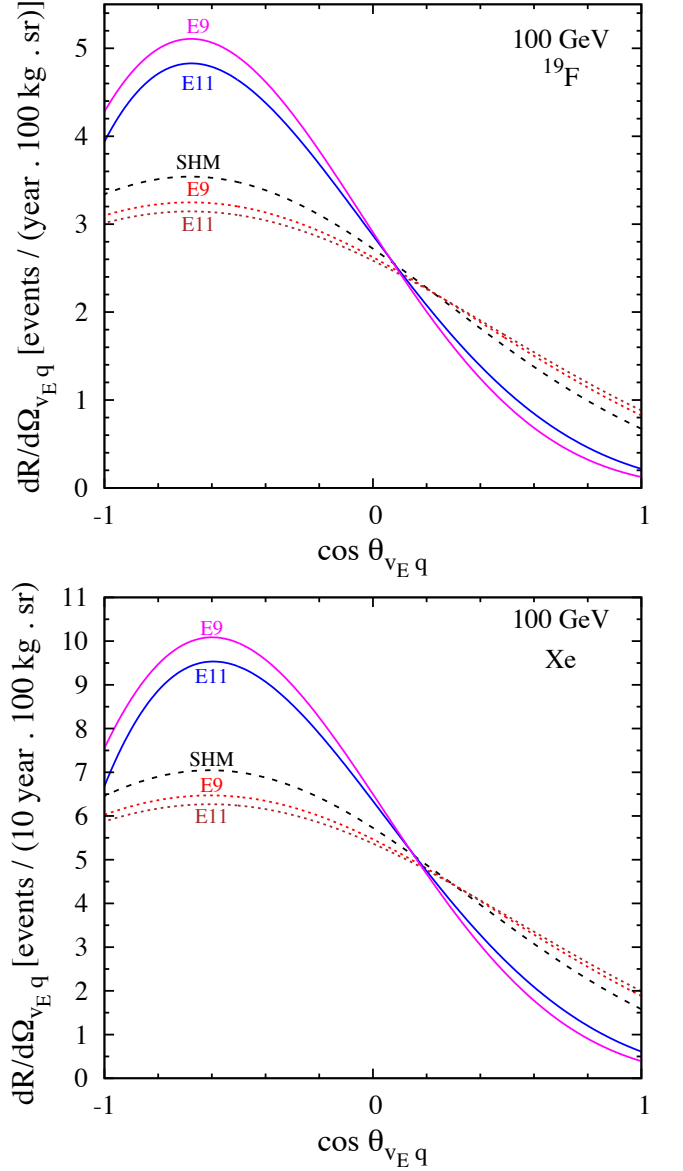


FIG. 2. The differential angular nuclear recoil spectrum for different Milky Way dark matter velocity distribution. The velocity profiles considered are the Mao et al. profile (solid blue and solid magenta) fit to halos E9 and E11, the SHM velocity distribution (black dotted), and the standard Maxwellian fit (red dotted and brown dotted) fit to halos E9 and E11. The target in the top panel is  $^{19}\text{F}$ , and that in the bottom panel is Xe. We consider spin-dependent interactions for both this plots. The integrated energy range considered for  $^{19}\text{F}$  and Xe is [5, 10] keV, and [5, 20] keV respectively.

MeV and  $\sim 19.5$  MeV. The recoil momentum of the Xe nuclei falls between  $\sim 32$  MeV and  $\sim 72.4$  MeV.

The various features in a directional detection experiment can be understood by analyzing eqn. 8. The dependence on the angle,  $\theta_{v_{E}q}$ , arises through the first exponential term. The energy dependence arises through the spin-dependent form factor and the first exponential

term. However, the energy dependence of the spin-dependent form factor is weak, especially for the low nuclear recoil energy, and it can be approximated as 1.

The number of events in the forward region,  $\cos \theta_{v_E q} \leq 0$ , denoted by  $N_F$  is larger than that in the backward region,  $\cos \theta_{v_E q} \geq 0$  denoted by  $N_B$ . This simply follows from eqn. 8 where one can show that at a given energy and angle

$$\frac{\text{Forward differential rate}}{\text{Backward differential rate}} \approx \frac{e^{-\frac{(-v_E |\cos \theta_{v_E q}| + q/2\mu)^2}{2v_0^2}}}{e^{-\frac{(v_E |\cos \theta_{v_E q}| + q/2\mu)^2}{2v_0^2}}}. \quad (11)$$

In the above approximate expression, we have neglected the term  $\exp[-v_{\text{max}}^2/(2v_0^2)] \ll 1$ .

The position of the maximum of the angular recoil rate can be derived from the term  $\exp\left[-\frac{(v_E \cos \theta_{v_E q} + q/2\mu)^2}{2v_0^2}\right]$ . If  $q/2\mu < v_E$ , the maximum of the exponential happens when the numerator in the argument becomes zero. This happens at  $\cos \theta_{v_E q} = -q/(2\mu v_E)$  which gives the ‘‘ring angle’’. The condition for the ‘‘ring angle’’ also implies that the ring is visible for heavier dark matter masses and lower recoil energies. The contrast between the differential rate at the ring, and that at the  $\cos \theta_{v_E q} = 1$  can be analytically derived as

$$\text{Ring contrast} \approx \frac{1}{e^{-\frac{(v_E + q/2\mu)^2}{2v_0^2}}}. \quad (12)$$

This shows that dark matter velocity profiles with smaller  $v_0$  can produce a larger contrast in the ring.

An experimental detection of the forward backward asymmetry and the ring depends on both the sense recognition and the angular resolution of the directional detection experiment. Due to the small track length, these measurements are a big experimental challenge. Encouragingly, many directional detection experiments have published an experimentally measured angular resolution and the sense recognition threshold [68]. More experimental work is needed to demonstrate that the angular resolution is measurable and the sense recognition is possible at lower recoil energies.

The angular size of the ring depends on the target and the dark matter velocity distribution. Heavier dark matter particles produce rings with bigger angular size. We tabulate the range in the ring sizes for the two targets and the cosmological dark matter velocity distribution for halos E9 and E11 in Table I for dark matter particle masses between 100 GeV and 1 TeV. We find that a heavier target produces a larger ring size.

### III. RESULTS

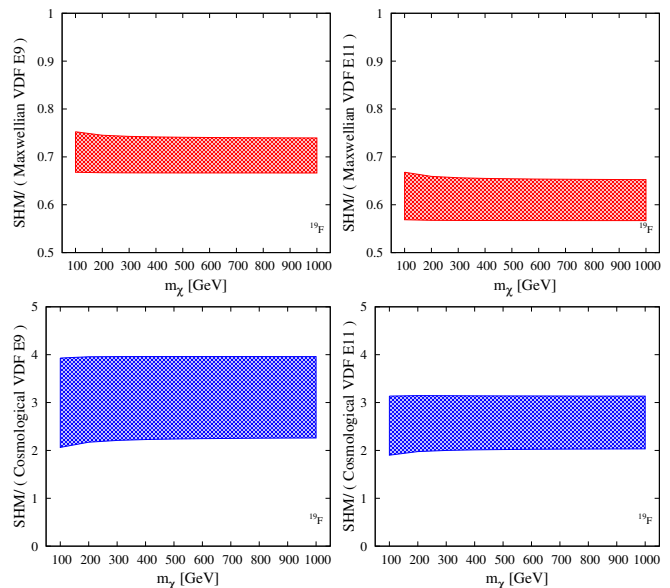


FIG. 3. Ratio of the number of events required (using different dark matter velocity profiles) for a  $3\sigma$  forward-backward discrimination using  $^{19}\text{F}$  target for various dark matter masses. The various ratios are (clockwise from top left): (i) SHM to Maxwellian VDF fit to E9, (ii) SHM to Maxwellian VDF fit to E11, (iii) SHM to Cosmological VDF fit to E11, and (iv) SHM to Cosmological VDF fit to E9.

In this section, we first show the nuclear recoil energy spectrum and then estimate the ratio of events to identify the forward-backward asymmetry and the ring at the  $3\sigma$  level.

In Fig. 2, we show the differential angular recoil rate when a dark matter particle of mass 100 GeV collides with a  $^{19}\text{F}$  and a Xe nucleus. The differential angular recoil rate when the dark matter velocity distribution follows the Mao et al. distribution are shown by solid blue and magenta lines. The differential angular recoil rate when the dark matter velocity distribution follows the standard Maxwellian distribution are shown by dotted red and brown lines. The differential angular recoil rate for the SHM is shown by the black dotted line. We integrate over the energy range [5, 10] keV for the  $^{19}\text{F}$  target, and over the energy range [5, 20] keV for the Xe target. Our choice of the energy range maximizes the contrast of the ring. A wider energy range

TABLE I. Range of the ring sizes for various targets and dark matter velocity distributions. The dark matter particle masses considered vary between 100 GeV and 1 TeV.

	SHM	E9 cosmological	E11 cosmological
$^{19}\text{F}$	$38^\circ - 44^\circ$	$40^\circ - 48^\circ$	$42^\circ - 51^\circ$
Xe	$44^\circ - 61^\circ$	$46^\circ - 72^\circ$	$49^\circ - 83^\circ$

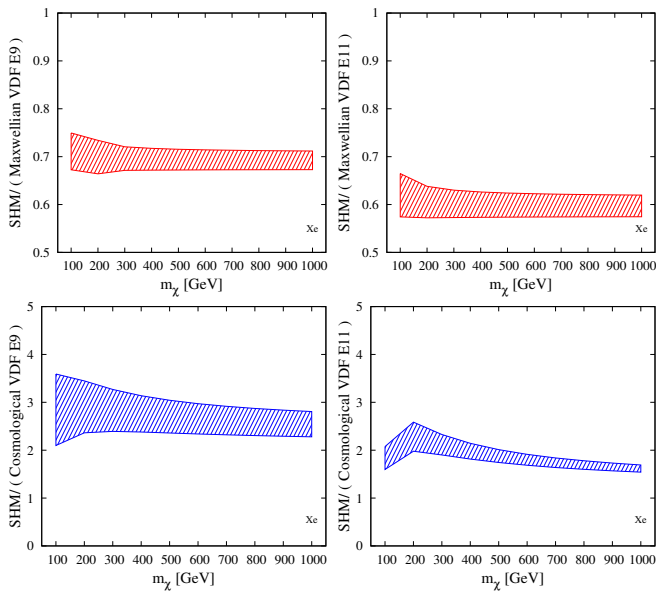


FIG. 4. Same as Fig. 3 but for Xe.

will increase the number of recoil events in the forward direction and thus the distinct bump-like feature of the ring is washed out. The local dark matter density is taken to be  $0.3 \text{ GeV}/\text{cm}^3$ , and the spin-dependent dark matter - nucleon cross section is taken to be  $10^{-40} \text{ cm}^2$  for both these figures. The angular recoil spectrum is directly proportional to this cross section and a smaller value will decrease it proportionately. The nuclear form factor is taken from Ref. [69].

The forward backward asymmetry is clearly visible for all the velocity profiles. The Mao et al. profile shows the most dramatic forward-backward asymmetry. The forward-backward asymmetry for the SHM and the standard Maxwellian distribution is weaker. This can be easily understood from Eqn. 11. The Mao et al. profile has a smaller “effective  $v_0$ ”, and hence a larger forward-backward asymmetry. The SHM and the standard Maxwellian have much larger  $v_0$ , and hence the contrast in their forward-backward asymmetry is much smaller.

The angle  $\theta_{v_{Eq}}$  at which the differential angular recoil rate is maximized is called the “ring” angle. As analytically explained in Eqn. 12, the Mao et al. profile fit produces the largest ring contrast, whereas the SHM and the standard Maxwellian profile fit produces a much weaker ring contrast.

We perform a simple statistical test [49] to determine the ratio of the number of events required for  $3\sigma$  discrimination for the forward-backward asymmetry for different dark matter velocity profiles. We also calculate the ratio of events for a  $3\sigma$  discovery of the ring for various different dark matter profiles. Using the ratio of events makes our results independent of the local dark matter density, dark matter - nucleon cross section, and many other uncertainties.

We briefly describe the procedure that we follow, and then describe the results. We calculate the number of events in the forward and backward direction by integrating over  $\theta_{v_{Eq}} \in [\pi/2, \pi]$  and  $\theta_{v_{Eq}} \in [0, \pi/2]$  respectively. We construct the forward-backward asymmetry as  $(N_F - N_B)/\sqrt{N_F + N_B}$ . We increase the exposure so that  $(N_F - N_B)/\sqrt{N_F + N_B} = 3$ . For this exposure, we calculate the total number of events for the given velocity distribution.

As expected from Fig. 2, the  $3\sigma$  discrimination in the forward-backward asymmetry is achieved with a smaller number of events for the Mao et al. velocity profile, whereas the standard Maxwellian fit to the halos E9 and E11 require the largest number of events for this discrimination. Fig. 3 shows the ratio of the number of events for various different input dark matter velocity profile required for such a discrimination with a  $^{19}\text{F}$  target. In the top panel, we plot the ratio of the number of events required in the SHM to that of the standard Maxwellian fit to halos E9 and E11 for various dark matter masses. The width of the bands are calculated taking the Poisson uncertainty in both the numerator and the denominator. It can be seen that the number of events required in the SHM is  $\sim 60\% - 70\%$  of that required in the standard Maxwellian velocity distribution function.

In the lower panel of Fig. 3, we show the ratio of the events required for the SHM velocity profile to the Mao et al. fit to the halos E9 and E11. Since the ring contrast is much larger for the Mao et al. fit to these halos, the number of events required for this discrimination is  $\sim 2 - 3$  times smaller than that required in SHM.

In Fig. 4, we show the same for Xe target. Even in this case, the Mao et al. fit to halos E9 and E11 require the least number of events to achieve the  $3\sigma$  discrimination in the forward-backward asymmetry. The bands representing the ratio has a smaller width compared to that of the  $^{19}\text{F}$  target. This is because the total number of events required for the  $3\sigma$  discrimination for Xe target is larger than that of  $^{19}\text{F}$  target.

We define the ring following Ref. [49]. The ring is defined to be between angles  $\theta_{v_{Eq1}} < \theta_{v_{Eq}} < \theta_{v_{Eq2}}$ , where

$$\frac{dR}{d\Omega_{v_{Eq1}}} = \frac{dR}{d\Omega_{v_{Eq2}}} = \frac{1}{2} \left( \frac{dR}{d\Omega_{v_{Eq}}}(\theta_{v_{Eq}} = \pi) + \frac{dR}{d\Omega_{v_{Eq}}} \Big|_{\max} \right). \quad (13)$$

For these two angles,  $\theta_{v_{Eq1}}$  and  $\theta_{v_{Eq2}}$ , we calculate the number of events inside these angles and between  $\theta_{v_{Eq2}}$  and  $\pi$ . We define  $N_{12} = \int_{\theta_{v_{Eq1}}}^{\theta_{v_{Eq2}}} d\Omega \frac{dR}{d\Omega_{v_{Eq}}}$ , and  $N_{2\pi} = \int_{\theta_{v_{Eq2}}}^{\pi} d\Omega \frac{dR}{d\Omega_{v_{Eq}}}$ . We calculate the exposure required such that  $(N_{12} - N_{2\pi})/\sqrt{N_{12} + N_{2\pi}} = 3$ . For such an exposure, we calculate the total number of events in the energy range [5, 10] keV for  $^{19}\text{F}$  and [5, 20] keV for Xe.

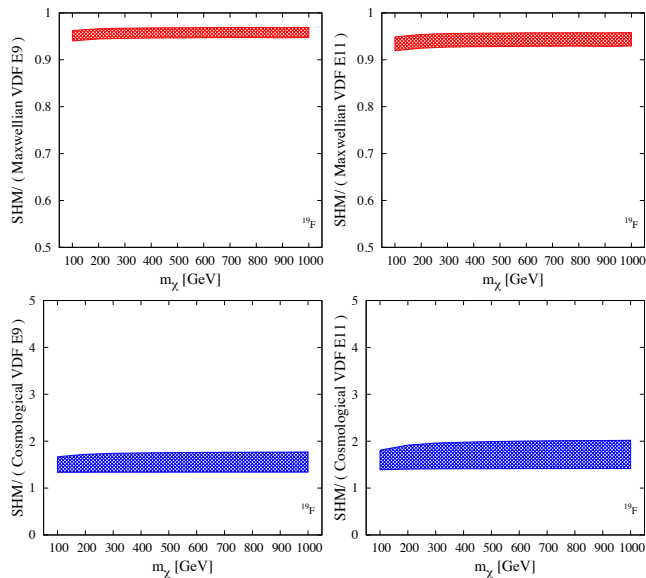


FIG. 5. Ratio of the number of events required (using different dark matter velocity profiles) for a  $3\sigma$  evidence of a ring using  $^{19}\text{F}$  target for various dark matter masses. The various ratios are (clockwise from top left): (i) SHM to Maxwellian VDF fit to E9, (ii) SHM to Maxwellian VDF fit to E11, (iii) SHM to Cosmological VDF fit to E11, and (iv) SHM to Cosmological VDF fit to E9.

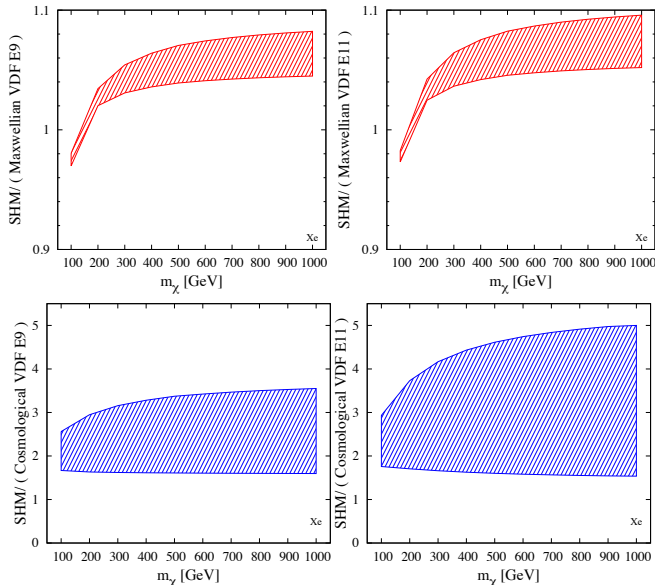


FIG. 6. Same as Fig. 5 but for Xe.

We find that using a factor of  $1/\sqrt{2}$  or  $1/3$  in eqn. 13 produces either a ring which is too small to be detected due to limitations imposed by angular resolution or a ring which is so thick that larger number of events are required for discovery.

The ratio of the number of events for the discrimination of the ring for various dark matter velocity profiles is shown in Figs. 5 and 6 for  $^{19}\text{F}$  and Xe target

respectively. The number of events required in the SHM for the ring discrimination (with  $^{19}\text{F}$  target) is very similar to the number of events required in the standard Maxwellian fit to the halos E9 and E11 (Fig. 5 top panel). The number of events required in a  $^{19}\text{F}$  target for the ring discrimination in the case of the Mao et al. profile is about a factor of 2 smaller than in the SHM (Fig. 5 bottom panel).

The corresponding figures for the Xe target is shown in Fig. 6. The number of events required for ring discrimination for SHM and standard Maxwellian fit to halos E9 and E11 are almost the same. The sharp downturn of the ratio reflects the fact that the reduced mass of the dark matter - Xe nucleus system changes a lot more slowly once the dark matter mass is greater than the mass of the relevant Xe nucleus. The number of events required for ring discrimination for the Mao et al. velocity distribution fit to halos E9 and E11 is  $\sim 2 - 3$  times smaller than that required for the SHM velocity distribution.

As explained earlier, it is possible to explain the results in this paper analytically by focusing on the “effective  $v_0$ ” of the dark matter velocity distribution. To explain the trend with varying  $v_0$ , we will now show the results for dark matter velocity distribution with different  $v_0$ . For example, the results obtained in this paper using the Mao et al., dark matter velocity distribution for the E9 halo can be well approximated by assuming an SHM velocity distribution with  $v_0 = 150 \text{ km s}^{-1}$ . For pedagogical purposes, we will now display our results for a dark matter velocity distribution following the SHM form with  $v_0 = 175 \text{ km s}^{-1}$  and  $v_0 = 200 \text{ km s}^{-1}$ . These are shown in Figs. 7 and 8. These ratios show that both the forward - backward ratio and the ring is more pronounced for a dark matter velocity profile with a smaller “effective  $v_0$ ” as analytically explained earlier. We want to remark that the two dark matter velocity distributions used in Figs. 7 and 8 are not derived from hydrodynamical simulations, but are used for explanatory purposes.

#### IV. CONCLUSION

Directional detection of dark matter is one of the most promising ways to unambiguously detect dark matter. Although present constraints are weak, it is expected that near future technological progress will make them more competitive. It has been pointed out that the forward-backward asymmetry and the ring-like structure of the maximum recoil rate can be used as an efficient discriminator between signal and background.

Recent hydrodynamical simulations have shown that the dark matter velocity profile differs substantially from the Standard Halo Model. We consider the SHM, the Mao et al. fit and the Maxwellian fit to halos E9 and E11 from the EAGLE HR and the APOSTLE IR simulations (see Fig. 1). The Mao et al. fit has a larger and smaller

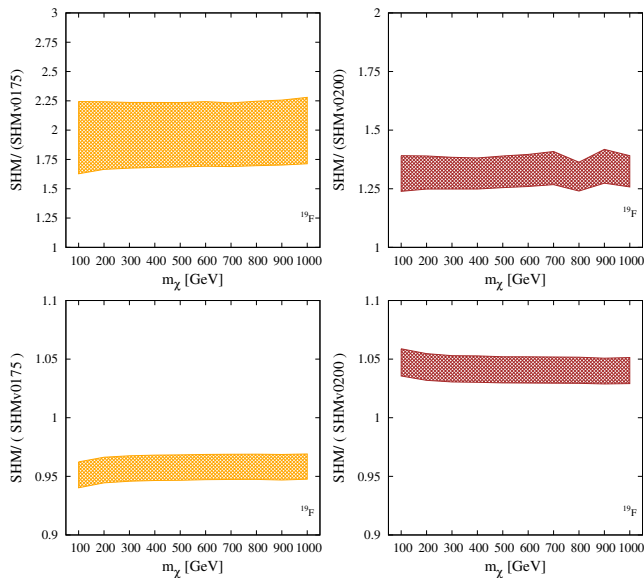


FIG. 7. Ratio of the number of events required (using different dark matter velocity profiles) for a  $3\sigma$  evidence of a forward-backward asymmetry (top panel) and a ring (bottom panel) using  $^{19}\text{F}$  target for various dark matter masses. The ratios for the plots on the left are for SHM with  $v_0 = 220 \text{ km s}^{-1}$  to SHM with  $v_0 = 175 \text{ km s}^{-1}$ . The ratios for the plots on the right are for SHM with  $v_0 = 220 \text{ km s}^{-1}$  to SHM with  $v_0 = 175 \text{ km s}^{-1}$ .

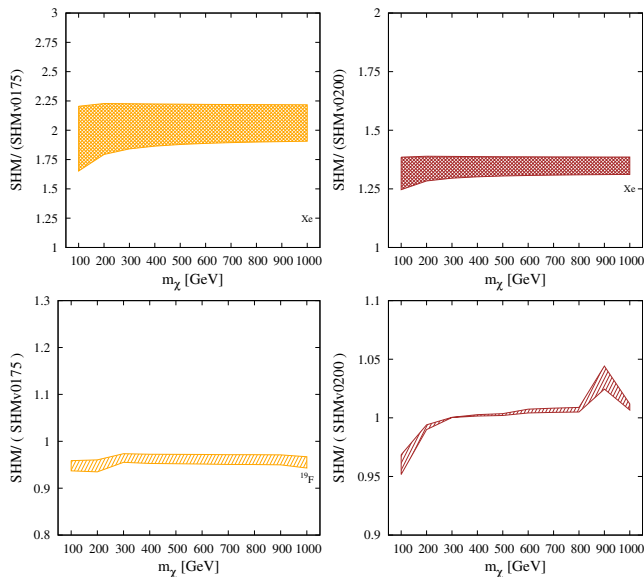


FIG. 8. Same as Fig. 7 but for Xe.

number of dark matter particles at low and high velocities respectively.

The effect of these different velocity profiles is shown in Fig. 2 for the  $^{19}\text{F}$  and Xe nuclei. The Mao et al. profile shows a much more distinct forward-backward asymmetry and consequently the presence of a ring. It is evident from this figure that fewer events will be required to estimate the forward-backward asymmetry and the presence of a ring when the Mao et al. dark matter velocity profile is considered.

The ratio of the number of events required for the discrimination of the forward-backward asymmetry and the ring is shown in Figs. 3, 4, 5 and 6. The number of events required for a  $3\sigma$  determination of the forward-backward asymmetry and for the evidence of a ring for the Mao et al. profile is  $\sim 2$ -3 times less than that for SHM for both  $^{19}\text{F}$  and Xe target.

It is important to use realistic dark matter velocity distributions while interpreting dark matter direct detection experiments. In this work we studied the impact of these velocity distributions on directional dark matter experiments. The realistic dark matter velocity distributions produce a much more dramatic forward-backward asymmetry in these experiments. The ring of the maximum dark matter recoil rate is also much more prominent if the Mao et al. velocity distribution is realized in nature. Along with other detection modes of dark matter (see for e.g., [70–75]), we hope that the use of these realistic dark matter velocity distributions will improve our understanding of the dark sector physics.

## ACKNOWLEDGMENTS

We thank Yao-Yuan Mao and Risa Wechsler for discussion. R.L. is supported by DOE Contract DE-AC02-76SF00515.

[1] **Planck** Collaboration, P. Ade *et al.*, “Planck 2015 results. XIII. Cosmological parameters”, [arXiv:1502.01589](https://arxiv.org/abs/1502.01589).

[2] G. Steigman, “Primordial Nucleosynthesis in the Precision Cosmology Era”, *Ann.Rev.Nucl.Part.Sci.* **57** (2007) 463–491, [arXiv:0712.1100](https://arxiv.org/abs/0712.1100).

- [3] L. E. Strigari, C. S. Frenk, and S. D. M. White, “Dynamical models for the Sculptor dwarf spheroidal in a Lambda CDM universe”, [arXiv:1406.6079](#).
- [4] P. Bhattacharjee, S. Chaudhury, S. Kundu, and S. Majumdar, “Sizing-up the WIMPs of Milky Way : Deriving the velocity distribution of Galactic Dark Matter particles from the rotation curve data”, *Phys.Rev.* **D87** (2013) 083525, [arXiv:1210.2328](#).
- [5] T. Marrodn Undagoitia and L. Rauch, “Dark matter direct-detection experiments”, *J. Phys.* **G43** (2016), no. 1, 013001, [arXiv:1509.08767](#).
- [6] G. Busoni *et al.*, “Recommendations on presenting LHC searches for missing transverse energy signals using simplified  $s$ -channel models of dark matter”, [arXiv:1603.04156](#).
- [7] M. Klasen, M. Pohl, and G. Sigl, “Indirect and direct search for dark matter”, *Prog. Part. Nucl. Phys.* **85** (2015) 1–32, [arXiv:1507.03800](#).
- [8] R. Catena and P. Ullio, “The local dark matter phase-space density and impact on WIMP direct detection”, *JCAP* **1205** (2012) 005, [arXiv:1111.3556](#).
- [9] J. Herrero-Garcia, “Halo-independent tests of dark matter annual modulation signals”, *JCAP* **1509** (2015), no. 09, 012, [arXiv:1506.03503](#).
- [10] E. Del Nobile, G. B. Gelmini, A. Georgescu, and J.-H. Huh, “Reevaluation of spin-dependent WIMP-proton interactions as an explanation of the DAMA data”, *JCAP* **1508** (2015), no. 08, 046, [arXiv:1502.07682](#).
- [11] R. Catena, A. Ibarra, and S. Wild, “DAMA confronts null searches in the effective theory of dark matter-nucleon interactions”, *JCAP* **1605** (2016), no. 05, 039, [arXiv:1602.04074](#).
- [12] S. Scopel and K.-H. Yoon, “Inelastic dark matter with spin-dependent couplings to protons and large modulation fractions in DAMA”, *JCAP* **1602** (2016), no. 02, 050, [arXiv:1512.00593](#).
- [13] K.-C. Yang, “Fermionic Dark Matter through a Light Pseudoscalar Portal: Hints from the DAMA Results”, *Phys. Rev.* **D94** (2016), no. 3, 035028, [arXiv:1604.04979](#).
- [14] D. N. Spergel, “The Motion of the Earth and the Detection of Wimps”, *Phys.Rev.* **D37** (1988) 1353.
- [15] C. J. Copi, J. Heo, and L. M. Krauss, “Directional sensitivity, WIMP detection, and the galactic halo”, *Phys.Lett.* **B461** (1999) 43–48, [arXiv:hep-ph/9904499](#).
- [16] C. J. Copi and L. M. Krauss, “Angular signatures for galactic halo WIMP scattering in direct detectors: Prospects and challenges”, *Phys.Rev.* **D63** (2001) 043507, [arXiv:astro-ph/0009467](#).
- [17] P. Gondolo, “Recoil momentum spectrum in directional dark matter detectors”, *Phys.Rev.* **D66** (2002) 103513, [arXiv:hep-ph/0209110](#).
- [18] B. Morgan, A. M. Green, and N. J. Spooner, “Directional statistics for WIMP direct detection”, *Phys.Rev.* **D71** (2005) 103507, [arXiv:astro-ph/0408047](#).
- [19] J. Billard, F. Mayet, J. Macias-Perez, and D. Santos, “Directional detection as a strategy to discover galactic Dark Matter”, *Phys.Lett.* **B691** (2010) 156–162, [arXiv:0911.4086](#).
- [20] S. Ahlen, N. Afshordi, J. Battat, J. Billard, N. Bozorgnia, *et al.*, “The case for a directional dark matter detector and the status of current experimental efforts”, *Int.J.Mod.Phys.* **A25** (2010) 1–51, [arXiv:0911.0323](#).
- [21] A. M. Green and B. Morgan, “The median recoil direction as a WIMP directional detection signal”, *Phys.Rev.* **D81** (2010) 061301, [arXiv:1002.2717](#).
- [22] S. K. Lee and A. H. Peter, “Probing the Local Velocity Distribution of WIMP Dark Matter with Directional Detectors”, *JCAP* **1204** (2012) 029, [arXiv:1202.5035](#).
- [23] P. Grothaus, M. Fairbairn, and J. Monroe, “Directional Dark Matter Detection Beyond the Neutrino Bound”, *Phys.Rev.* **D90** (2014), no. 5, 055018, [arXiv:1406.5047](#).
- [24] C. A. J. O’Hare and A. M. Green, “Directional detection of dark matter streams”, *Phys.Rev.* **D90** (2014), no. 12, 123511, [arXiv:1410.2749](#).
- [25] C. A. J. O’Hare, A. M. Green, J. Billard, E. Figueroa-Feliciano, and L. E. Strigari, “Readout strategies for directional dark matter detection beyond the neutrino background”, *Phys. Rev.* **D92** (2015), no. 6, 063518, [arXiv:1505.08061](#).
- [26] R. Laha, “Directional detection of dark matter in universal bound states”, *Phys. Rev.* **D92** (2015) 083509, [arXiv:1505.02772](#).
- [27] F. Mayet *et al.*, “A review of the discovery reach of directional Dark Matter detection”, *Phys. Rept.* **627** (2016) 1–49, [arXiv:1602.03781](#).
- [28] B. J. Kavanagh, “Discretising the velocity distribution for directional dark matter experiments”, [arXiv:1502.04224](#).
- [29] B. J. Kavanagh and C. A. J. O’Hare, “Reconstructing the three-dimensional local dark matter velocity distribution”, [arXiv:1609.08630](#).
- [30] E. Daw *et al.*, “The DRIFT Directional Dark Matter Experiments”, *EAS Publ. Ser.* **53** (2012) 11–18, [arXiv:1110.0222](#).
- [31] **DRIFT Collaboration** Collaboration, J. Battat *et al.*, “First background-free limit from a directional dark matter experiment: results from a fully fiducialised DRIFT detector”, [arXiv:1410.7821](#).
- [32] I. Jaegle, H. Feng, S. Ross, J. Yamaoka, S. E. Vahsen, H. Feng, S. Ross, J. Yamaoka, and S. E. Vahsen, “Simulation of the Directional Dark Matter Detector ( $D^3$ ) and Directional Neutron Observer (DiNO)”, *EAS Publ. Ser.* **53** (2012) 111–118, [arXiv:1110.3444](#).
- [33] S. Vahsen, H. Feng, M. Garcia-Sciveres, I. Jaegle, J. Kadyk, *et al.*, “The Directional Dark Matter Detector ( $D^3$ )”, *EAS Publ.Ser.* **53** (2012) 43–50, [arXiv:1110.3401](#).
- [34] **DMTPC Collaboration** Collaboration, J. Monroe, “Status and Prospects of the DMTPC Directional Dark Matter Experiment”, *EAS Publ.Ser.* **53** (2012) 19–24.
- [35] **DMTPC** Collaboration, J. Monroe, “Status and Prospects of the DMTPC Directional Dark Matter Experiment”, *AIP Conf. Proc.* **1441** (2012) 515–517, [arXiv:1111.0220](#).
- [36] **DMTPC** Collaboration, M. Leyton, “Directional dark matter detection with the DMTPC  $m^3$  experiment”, *J. Phys. Conf. Ser.* **718** (2016), no. 4, 042035.
- [37] K. Miuchi *et al.*, “First underground results with NEWAGE-0.3a direction-sensitive dark matter detector”, *Phys. Lett.* **B686** (2010) 11–17, [arXiv:1002.1794](#).
- [38] K. Nakamura, K. Miuchi, S. Iwaki, H. Kubo, T. Mizumoto, *et al.*, “NEWAGE”, *J.Phys. Conf.Ser.* **375** (2012) 012013, [arXiv:1109.3099](#).



- [39] Q. Riffard, J. Billard, G. Bosson, O. Bourrion, O. Guillaudin, *et al.*, “Dark Matter directional detection with MIMAC”, [arXiv:1306.4173](#).
- [40] Q. Riffard *et al.*, “MIMAC low energy electron-recoil discrimination measured with fast neutrons”, *JINST* **11** (2016), no. 08, P08011, [arXiv:1602.01738](#).
- [41] T. Naka and K. Miuchi, eds., *Proceedings, 4th Workshop on Directional Detection of Dark Matter (CYGNUS 2013)*, vol. 469. 2013.
- [42] F. Cappella *et al.*, “On the potentiality of the  $ZnWO_4$  anisotropic detectors to measure the directionality of Dark Matter”, *Eur. Phys. J.* **C73** (2013), no. 1, 2276.
- [43] L. M. Capparelli, G. Cavoto, D. Mazzilli, and A. D. Polosa, “Directional Dark Matter Searches with Carbon Nanotubes”, *Phys. Dark Univ.* **9-10** (2015) 24–30, [arXiv:1412.8213](#), [Erratum: *Phys. Dark Univ.* **11**, 79(2016)].
- [44] NEWS Collaboration, A. Aleksandrov *et al.*, “NEWS: Nuclear Emulsions for WIMP Search”, [arXiv:1604.04199](#).
- [45] D. Nygren, “Columnar recombination: a tool for nuclear recoil directional sensitivity in a xenon-based direct detection WIMP search”, *J.Phys.Conf.Ser.* **460** (2013) 012006.
- [46] V. Gehman, A. Goldschmidt, D. Nygren, C. Oliveira, and J. Renner, “A plan for directional dark matter sensitivity in high-pressure xenon detectors through the addition of wavelength shifting gaseous molecules”, *JINST* **8** (2013) C10001.
- [47] G. Mohlabeng, K. Kong, J. Li, A. Para, and J. Yoo, “Dark Matter Directionality Revisited with a High Pressure Xenon Gas Detector”, [arXiv:1503.03937](#).
- [48] J. Li, “Directional dark matter by polar angle direct detection and application of columnar recombination”, [arXiv:1503.07320](#).
- [49] N. Bozorgnia, G. B. Gelmini, and P. Gondolo, “Ring-like features in directional dark matter detection”, *JCAP* **1206** (2012) 037, [arXiv:1111.6361](#).
- [50] R. Laha and E. Braaten, “Direct detection of dark matter in universal bound states”, *Phys.Rev.* **D89** (2014), no. 10, 103510, [arXiv:1311.6386](#).
- [51] F. S. Ling, E. Nezri, E. Athanassoula, and R. Teyssier, “Dark Matter Direct Detection Signals inferred from a Cosmological N-body Simulation with Baryons”, *JCAP* **1002** (2010) 012, [arXiv:0909.2028](#).
- [52] M. Kuhlen, A. Pillepich, J. Guedes, and P. Madau, “The Distribution of Dark Matter in the Milky Way’s Disk”, *Astrophys. J.* **784** (2014) 161, [arXiv:1308.1703](#).
- [53] I. Butsky, A. V. Maccio, A. A. Dutton, L. Wang, G. S. Stinson, C. Penzo, X. Kang, B. W. Keller, and J. Wadsley, “NIHAO project II: Halo shape, phase-space density and velocity distribution of dark matter in galaxy formation simulations”, [arXiv:1503.04814](#).
- [54] N. Bozorgnia, F. Calore, M. Schaller, M. Lovell, G. Bertone, C. S. Frenk, R. A. Crain, J. F. Navarro, J. Schaye, and T. Theuns, “Simulated Milky Way analogues: implications for dark matter direct searches”, *JCAP* **1605** (2016), no. 05, 024, [arXiv:1601.04707](#).
- [55] C. Kelso, C. Savage, M. Valluri, K. Freese, G. S. Stinson, and J. Bailin, “The impact of baryons on the direct detection of dark matter”, *JCAP* **1608** (2016) 071, [arXiv:1601.04725](#).
- [56] J. D. Sloane, M. R. Buckley, A. M. Brooks, and F. Governato, “Assessing Astrophysical Uncertainties in Direct Detection with Galaxy Simulations”, [arXiv:1601.05402](#).
- [57] M. S. Petersen, N. Katz, and M. D. Weinberg, “The Dynamical Response of Dark Matter to Galaxy Evolution Affects Direct-Detection Experiments”, [arXiv:1609.01307](#).
- [58] T. Piffl *et al.*, “The RAVE survey: the Galactic escape speed and the mass of the Milky Way”, *Astron. Astrophys.* **562** (2014) A91, [arXiv:1309.4293](#).
- [59] J. Schaye *et al.*, “The EAGLE project: Simulating the evolution and assembly of galaxies and their environments”, *Mon. Not. Roy. Astron. Soc.* **446** (2015) 521–554, [arXiv:1407.7040](#).
- [60] R. A. Crain *et al.*, “The EAGLE simulations of galaxy formation: calibration of subgrid physics and model variations”, *Mon. Not. Roy. Astron. Soc.* **450** (2015), no. 2, 1937–1961, [arXiv:1501.01311](#).
- [61] T. Sawala *et al.*, “The APOSTLE simulations: solutions to the Local Group’s cosmic puzzles”, *Mon. Not. Roy. Astron. Soc.* **457** (2016), no. 2, 1931–1943, [arXiv:1511.01098](#).
- [62] A. Fattahi, J. F. Navarro, T. Sawala, C. S. Frenk, K. A. Oman, R. A. Crain, M. Furlong, M. Schaller, J. Schaye, T. Theuns, and A. Jenkins, “The APOSTLE project: Local Group kinematic mass constraints and simulation candidate selection”, *Monthly Notices of the Royal Astronomical Society* **457** (2016) 844–856, [arXiv:1507.03643](#).
- [63] Y.-Y. Mao, L. E. Strigari, R. H. Wechsler, H.-Y. Wu, and O. Hahn, “Halo-to-Halo Similarity and Scatter in the Velocity Distribution of Dark Matter”, *Astrophys. J.* **764** (2013) 35, [arXiv:1210.2721](#).
- [64] M. Lisanti, L. E. Strigari, J. G. Wacker, and R. H. Wechsler, “The Dark Matter at the End of the Galaxy”, *Phys. Rev.* **D83** (2011) 023519, [arXiv:1010.4300](#).
- [65] F. Calore, N. Bozorgnia, M. Lovell, G. Bertone, M. Schaller, C. S. Frenk, R. A. Crain, J. Schaye, T. Theuns, and J. W. Trayford, “Simulated Milky Way analogues: implications for dark matter indirect searches”, *JCAP* **1512** (2015), no. 12, 053, [arXiv:1509.02164](#).
- [66] R. Catena, “Dark matter directional detection in non-relativistic effective theories”, *JCAP* **1507** (2015), no. 07, 026, [arXiv:1505.06441](#).
- [67] B. J. Kavanagh, “New directional signatures from the nonrelativistic effective field theory of dark matter”, *Phys. Rev.* **D92** (2015), no. 2, 023513, [arXiv:1505.07406](#).
- [68] J. B. R. Battat *et al.*, “Readout technologies for directional WIMP Dark Matter detection”, *Phys. Rept.* **662** (2016) 1–46, [arXiv:1610.02396](#).
- [69] V. A. Bednyakov and F. Simkovic, “Nuclear spin structure in dark matter search: The Finite momentum transfer limit”, *Phys. Part. Nucl.* **37** (2006) S106–S128, [arXiv:hep-ph/0608097](#).
- [70] B. Dasgupta and R. Laha, “Neutrinos in IceCube/KM3NeT as probes of Dark Matter Substructures in Galaxy Clusters”, *Phys. Rev.* **D86** (2012) 093001, [arXiv:1206.1322](#).

- [71] R. Laha, K. C. Y. Ng, B. Dasgupta, and S. Horiuchi, “Galactic center radio constraints on gamma-ray lines from dark matter annihilation”, *Phys. Rev.* **D87** (2013), no. 4, 043516, [arXiv:1208.5488](#).
- [72] K. C. Y. Ng, R. Laha, S. Campbell, S. Horiuchi, B. Dasgupta, K. Murase, and J. F. Beacom, “Resolving small-scale dark matter structures using multisource indirect detection”, *Phys. Rev.* **D89** (2014), no. 8, 083001, [arXiv:1310.1915](#).
- [73] K. Murase, R. Laha, S. Ando, and M. Ahlers, “Testing the Dark Matter Scenario for PeV Neutrinos Observed in IceCube”, *Phys. Rev. Lett.* **115** (2015), no. 7, 071301, [arXiv:1503.04663](#).
- [74] E. G. Speckhard, K. C. Y. Ng, J. F. Beacom, and R. Laha, “Dark Matter Velocity Spectroscopy”, *Phys. Rev. Lett.* **116** (2016), no. 3, 031301, [arXiv:1507.04744](#).
- [75] D. Chowdhury, A. M. Iyer, and R. Laha, “Constraints on dark matter annihilation to fermions and a photon”, [arXiv:1601.06140](#).